Comparative study of strong-field ionization of alkaline-earth-metal atoms

HuiPeng Kang,[1,2,3] Shi Chen,[4,5] ZhiYang Lin,[6] Wei Chu,[7] JinPing Yao,[7] Wei Quan,[3] Jing Chen,[8,9,*] XiaoJun Liu,[3,†] Ya Cheng,[7,10,‡] and ZhiZhan Xu[7]

[1]*Institute of Optics and Quantum Electronics, Friedrich Schiller University Jena, Max-Wien-Platz 1, 07743 Jena, Germany*
[2]*Helmholtz Institut Jena, Frötbelstieg 3, 07743 Jena, Germany*
[3]*State Key Laboratory of Magnetic Resonance and Atomic and Molecular Physics, Wuhan Institute of Physics and Mathematics, Innovation Academy for Precision Measurement Science and Technology, Chinese Academy of Sciences, Wuhan 430071, China*
[4]*School of Physics, Peking University, Beijing 100871, China*
[5]*HEDPS, Center for Applied Physics and Technology, Peking University, Beijing 100871, China*
[6]*Fujian Key Laboratory of Light Propagation and Transformation, College of Information Science and Engineering, Huaqiao University, Xiamen 361021, China*
[7]*State Key Laboratory of High Field Laser Physics, Shanghai Institute of Optics and Fine Mechanics, Chinese Academy of Sciences, Shanghai 201800, China*
[8]*Institute of Applied Physics and Computational Mathematics, P.O. Box 8009, Beijing 100088, China*
[9]*Center for Advanced Material Diagnostic Technology, College of Engineering Physics, Shenzhen Technology University, Shenzhen 518118, China*
[10]*State Key Laboratory of Precision Spectroscopy, East China Normal University, Shanghai 200062, China*

(Received 26 November 2019; accepted 1 May 2020; published 22 May 2020)

We report on a comparative study of strong-field ionization of alkaline-earth-metal atoms by intense femtosecond laser pulses from near-infrared to midinfrared wavelengths. By collecting the ionization signals only produced within the central portion of the laser focus, the focus volume effect is largely reduced and the saturation intensities for different alkaline-earth-metal atoms are reliably determined, which permits us to directly test the strong-field-ionization theories. We demonstrate that the Perelomov-Popov-Terent'ev model accurately predicts the experimental ionization yields and saturation intensities in general for arbitrary values of the Keldysh parameter, while the Ammosov-Delone-Krainov simulations agree with the experiments for the tunneling-ionization regime and also for the regime when the Keldysh parameter is around 1. Our work presents benchmark data for strong-field ionization of alkaline-earth metals over a broad range of laser parameters and confirms the validity of Keldysh's picture for such atoms.

DOI: 10.1103/PhysRevA.101.053433

I. INTRODUCTION

Above-threshold ionization (ATI) is one of the most fundamental nonlinear processes for atoms and molecules interacting with intense laser pulses. It refers to the liberation of an electron bound in the atomic or molecular target with absorption of many more photons than the minimum number required to overcome the ionization potential (for reviews, see [1,2]). Since its discovery 40 years ago [3], ATI has continued to attract intense experimental and theoretical attention and renew our understanding of strong-field physics. It was also demonstrated that ATI has various important applications such as probing the ultrafast dynamics of atoms and molecules [4–6] and characterization of the carrier-envelope phase of few-cycle laser pulses [7].

It is now widely accepted that the ATI process is dominated by multiphoton ionization (MPI) or tunneling ionization (TI) depending on the Keldysh parameter $\gamma = \omega\sqrt{2I_p}/E$ (in atomic units), based on Keldysh's seminal work [8]. Here I_p is the ionization potential and E and ω are the laser electric-field amplitude and frequency, respectively. According to Keldysh's rate [8], for the MPI regime where $\gamma \gg 1$, the total ionization rate of ATI is proportional to $(E/w)^{2I_p/\hbar\omega}$, while for the TI regime where $\gamma \ll 1$, the total ionization rate scales exponentially with the laser field. Subsequently, Perelomov *et al.* derived the exact form of the preexponential factor of Keldysh's rate [9]. This is the well-known Perelomov-Popov-Terent'ev (PPT) formula. The PPT theory is shown to be valid for arbitrary values of γ and laser wavelength [10]. A more commonly employed theory in the strong-field physics community is the Ammosov-Delone-Krainov (ADK) model [11]. This model accounts for the static-field ionization rate of arbitrary atoms and atomic ions and is thus applicable usually for $\gamma \to 0$ (the TI regime).

One way to experimentally test the strong-field-ionization theory is to scrutinize the ionization yield as a function of laser intensity. Such experiments have been intensively performed mainly on rare-gas atoms with near-infrared lasers (see, e.g., [12–16]). The findings support Keldysh's picture. It was also found that the ADK model works well even for the transition regime between MPI and TI ($\gamma \sim 1$). However,

*chen_jing@iapcm.ac.cn
†xjliu@wipm.ac.cn
‡ya.cheng@siom.ac.cn

strong-field-ionization experiments on other atomic species have been performed much less frequently. Only a few investigations along this direction have been carried out (see, e.g., [17–20]). For instance, several transition-metal atoms have been systematically studied and the experiments showed a dramatic suppression of the ionization yield with respect to the prediction from the ADK theory [19], which can be attributed to the dynamic screening effects within the transition-metal atoms. Recently, an experimental investigation across various atomic targets including Na, K, Zn, and Mg was reported in [21]. It revealed the general sufficiency of the PPT theoretical prediction and the limitation of the ADK theory for small-γ values.

In a realistic experiment, the measured ionization yields are usually the results of integration over three-dimensional ion distributions produced within the laser focus volume. Therefore, the ionization yields are averaged over a broad range of intensities largely depending on the realistic laser focus. This focus volume effect can smear out many subtle features and thus introduces uncertainty in the theoretical interpretation of the experiment. Over the past decades, various methods have been proposed to circumvent this spatial-averaging effect [22–26]. Typical ways are, e.g., to reduce the focus volume [27] or implementing weaker focusing [28]. Indeed, characteristic features such as interference [29] and charge-state depletion effects [30] in multiple ionization of Xe, which have escaped observation with the traditional geometry of laser focus, have been revealed by employing these methods. In particular, Hansch and Van Woerkom [30] introduced an intensity-selective scanning technique in which the collected ionization products are limited to a small portion of the interaction volume by an aperture so that the intensity variation along the beam direction is removed.

In contrast, alkaline-earth-metal atoms have shown interesting features when ionized by a strong laser field [18,31–36]. Ionization yield measurements using nanosecond or picosecond laser pulses have been performed mainly in the MPI regime so far [37–39] and it remains unclear whether the widely used strong-field-ionization theories are applicable for such atoms (except for Mg [21]), which is of fundamental importance to understanding their ionization dynamics. Although the PPT and ADK theories have been compared with the full-volume ionization measurements on Mg in Ref. [21], it is unclear whether the conclusion on Mg can be generalized to other alkaline-earth metals. This is mainly because, first, strong-field ionization of alkaline-earth metals has shown strong target-dependent behaviors. For example, different single- and double-ionization channels for different alkaline-earth metals have been experimentally revealed [37,40,41]. Second, it has been realized in Ref. [19] that the dynamical polarization effect can lead to obvious discrepancies between the experiments and the ADK theory. As compared with the transition metals studied in Ref. [19], alkaline-earth metals also have high polarizabilities. Although no obvious polarization effects can be found for Mg results in Ref. [21], other alkaline-earth metals can have much larger polarizabilities (e.g., 272.1 a.u. for Ba) than that of Mg (71.3 a.u.) [42]. Obviously, the conclusion on Mg in Ref. [21] cannot be simply extended to other alkaline-earth metals without further experimental studies. Therefore, it is very crucial to study different alkaline-earth metals *with the same laser parameters* and test if their ionization yields can be described by the PPT and ADK theories.

In this paper we present a systematic study of strong-field ionization of alkaline-earth-metal atoms (Mg, Ca, Sr, and Ba) using intense femtosecond laser pulses from near-infrared to midinfrared wavelengths. Therefore, we explore their ionization dynamics from MPI to the deep TI regime. Using a narrow slit orthogonal to the laser-beam direction, only the ionization yields produced within the central portion of the laser focus are detected. This enables us to largely reduce the focus volume effect when testing strong-field-ionization theory. Additionally, it allows us to reliably determine the saturation intensity [43,44], which can be unambiguously compared with theory. Furthermore, we mix different alkaline-earth metals in the atomic beam in our experiments. This permits a comparative study of ionization dynamics of different alkaline-earth metals under identical laser conditions. We find that the ionization saturation is very similar for Ca and Sr due to their very close ionization potentials, while the ionization saturation is much easier for Ba as compared with Mg. We compare the measured ion yields, saturation intensities for different alkaline-earth-metal atoms, and the PPT and ADK theoretical simulations. We find overall good agreement with the PPT prediction for arbitrary values of γ. The ADK simulation is found to agree well with the experiments in the TI regime and also in the intermediate regime when γ is around 1. Our work presents benchmark data for strong-field ionization of alkaline-earth-metal atoms over a broad range of laser parameters and verifies the validity of Keldysh's picture for those atoms.

This paper is organized as follows. In Sec. II we introduce the experimental apparatus. The PPT and ADK theories are described briefly in Sec. III. In Sec. IV we present and discuss the results. A summary and conclusions are given in Sec. V.

II. EXPERIMENTAL SETUP

In our experiments, an optical parametric amplifier (OPA, TOPAS-C, Light Conversion, Inc.), pumped by a commercial Ti:sapphire laser system (2.5 mJ, 45 fs, 1 kHz, Legend, Coherent, Inc.), is employed to generate wavelength tunable midinfrared femtosecond laser pulses. Using a combination of an achromatic half waveplate and a polarizer, the pulse energy is variable before being focused into the vacuum chamber. A homemade time-of-flight (TOF) mass spectrometer is used for detecting the ion signals. Figure 1 depicts schematically our spectrometer. The base pressure achieved in the chamber is below 10^{-8} mbar. The measurements are performed with a 1-cm extraction region and a ~45-cm field-free drift region. Due to the larger beam size used for 2000-nm pulses, the focused waists in the present experiments are 8.49, 15.9, and 13.2 μm for 800, 1500, and 2000 nm, respectively. The corresponding confocal parameters (twice the Rayleigh length) are 0.56, 1.06, and 0.54 mm, respectively. A 0.5-mm grounded metal slit, which is orthogonal to both the laser propagation direction (z axis) and the TOF axis (x axis), is placed at the entrance to the drift region. The slit limits the collection of ions to those resulting from the beam waist with a parallel

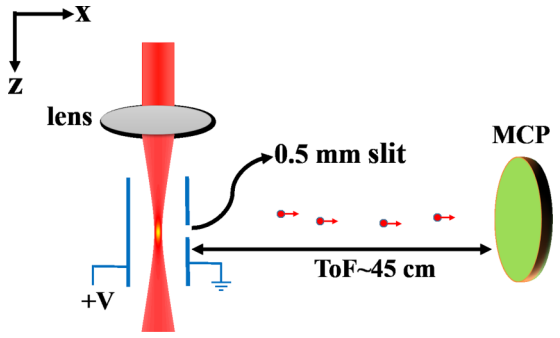

FIG. 1. Schematic of the main part of our time-of-flight mass spectrometer.

beam geometry, thus cutting off the intensity variation over the spatial region for large-z values.

An electrically heated stainless atomic oven is used to produce a collimated atomic beam. To suppress the systematic uncertainties originating from the absolute determination of the atomic target density and laser intensity, we mix Ba and Mg (Sr and Ca) in the atomic oven. Only the ions that fly through the slit are detected by a microchannel plate (MCP) located at the end of the spectrometer. The ion signal is then amplified, discriminated, and finally recorded by a multihit time digitizer to produce TOF mass spectra. The digitizer is able to count multiple events with a time resolution of 0.5 ns. During the measurements, the density of the mixture of two different atomic species, i.e., Ba and Mg (Sr and Ca), in the ionization volume remains stable by continuously monitoring the temperature of the oven and also the ion signals of the two atomic species separately. The laser peak intensities for each wavelength are determined by comparing the measured saturation intensity of the Xe^+ yield with the ADK calculation [45]. The uncertainty of the intensity determination is estimated to be about 10%.

III. THE PPT AND ADK THEORIES

The PPT ionization rate can be expressed as the sum of the rates of ATI corresponding to absorption of q photons

$$w_{\mathrm{PPT}}(E,\omega)=\sum_{q\geqslant q_{\min}}^{\infty} w_q(E,\omega), \tag{1}$$

where E and ω are the amplitude and frequency of the laser field, respectively, and $q_{\min}=(I_p+U_p)/\omega$ is the minimum number of photons required to overcome the effective ionization potential of the target, where I_p is the field-free ionization potential and U_p is the ponderomotive energy. After a series of derivations, the PPT rate can be written as [9]

$$\begin{aligned} w_{\mathrm{PPT}}(E,\omega)=&C^2_{n^*l^*}f(l,m)I_p\sqrt{\frac{6}{\pi}}\left(\frac{2}{En^{*3}}\right)^{2n^*-|m|-3/2}\\ &\times(1+\gamma^2)^{|m|/2+3/4}A_m(\omega,\gamma)\\ &\times\exp\left[-\frac{2(2I_p)^{3/2}}{3E}g(\gamma)\right], \end{aligned} \tag{2}$$

where $C^2_{n^*l^*}=\frac{2^{2n^*}}{n^*\Gamma(n^*+l^*+1)\Gamma(n^*-l^*)}$ and $f(l,m)=\frac{(2l+1)(l+|m|)!}{2^{|m|}(|m|)!(l-|m|)!}$. Here $n^*=\frac{1}{\sqrt{2I_p}}$ is the effective quantum number, $l^*=n^*-1$ is the effective orbital quantum number, and l and m are the orbital quantum number and magnetic quantum number, respectively. The factor $(2/En^{*3})^{2n^*}$ accounts for the long-range Coulomb potential effect [46]. Further, $\gamma=\frac{\omega\sqrt{2I_p}}{E}$ is the Keldysh parameter and

$$g(\gamma)=\frac{3}{2\gamma}\left[\left(1+\frac{1}{2\gamma^2}\right)\sinh^{-1}\gamma-\frac{\sqrt{1+\gamma^2}}{2\gamma}\right],$$

$$\begin{aligned} A_m(\omega,\gamma)=&\frac{4\gamma^2}{\sqrt{3\pi}|m|!(1+\gamma^2)}\\ &\times\sum_{q\geqslant q_{\min}}^{\infty}e^{-\alpha(\gamma)(q-\nu)}w_m(\sqrt{\beta(\gamma)(q-q_{\min})}), \end{aligned}$$

where $w_m(x)=\frac{x^{2|m|+1}}{2}\int_0^1\frac{e^{-x^2t}t^{|m|}}{\sqrt{1-t}}dt$, $\alpha(\gamma)=2(\sinh^{-1}\gamma-\frac{\gamma}{\sqrt{1+\gamma^2}})$, $\beta(\gamma)=\frac{2\gamma}{\sqrt{1+\gamma^2}}$, and $\nu=\frac{I_p}{\omega}(1+\frac{1}{2\gamma^2})$.

Under the adiabatic approximation $\gamma\ll 1$, the widely used ADK formula [11] for the ionization rate can be obtained from Eq. (2), which is given by

$$\begin{aligned} w_{\mathrm{ADK}}(E)=&C^2_{n^*l^*}f(l,m)I_p\sqrt{\frac{6}{\pi}}\left(\frac{2}{En^{*3}}\right)^{2n^*-|m|-3/2}\\ &\times e^{-2(2I_p)^{3/2}/3E}, \end{aligned} \tag{3}$$

where $C^2_{n^*l^*}=(\frac{2e}{n^*})^{n^*}\frac{1}{\sqrt{2\pi n^*}}$ with e constant can be derived when the condition $n^*\gg l^*$ is satisfied [11]. To calculate the ionization rate, we average over all the possible values of m:

$$W=\frac{1}{2l+1}\sum_{m=-l}^{l}w_{\mathrm{PPT(ADK)}}. \tag{4}$$

The ionization probability by a laser pulse at position (r,z) inside the laser focus can be calculated by

$$P=1-\exp\left(-\int_{-\infty}^{+\infty}W[E_{r,z}f(t)]dt\right), \tag{5}$$

where $E_{r,z}$ is the peak amplitude of the laser field at (r,z) and $f(t)$ is the pulse envelope having a Gaussian shape.

In our experiments, only ions between the 0.5-mm slit along the laser propagation (z axis) can be detected. Therefore, to compare with the data, the spatial distribution of the intensity limited by the z boundaries has to be considered. The volume inside an isointensity surface I_0 restricted between $-z_i$ and z_i (here $z_i=0.25$ mm) is [45]

$$\begin{aligned} V_{I>I_0}=V_0\Bigg[&\frac{2\zeta^3}{9}+\frac{4\zeta}{3}-\frac{4}{3}\tan^{-1}(\zeta)\\ &+\left(\frac{\zeta^3}{3}+\zeta\right)\ln\left(\frac{\xi^2+1}{\zeta^2+1}\right)\Bigg], \end{aligned} \tag{6}$$

where $V_0=\frac{\pi^2w_f^4}{\lambda}$, $\xi=\sqrt{\frac{I_{\mathrm{peak}}-I_0}{I_0}}$, and $\zeta=\xi$ for $\xi<z_i/z_r$ and z_i/z_r for $\xi\geqslant z_i/z_r$. Here λ is the laser wavelength, I_{peak} is the peak intensity, w_f is the focus waist, and z_r is the Rayleigh range. The total ionization yield is obtained by integrating P over the volume limited between $-z_i$ and z_i.

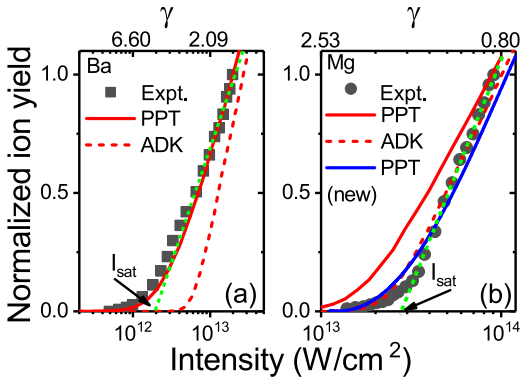

FIG. 2. Ion yields versus laser intensity for (a) Ba and (b) Mg. The black squares and circles are the experimental data that have been normalized to the point at the highest intensity. The corresponding Keldysh parameters are shown on the top. The red solid and dashed curves are the PPT and ADK simulations, respectively. The blue solid curve in (b) is the PPT simulation using the generalized Coulomb correction factor in [47]. The green straight dotted lines, which follow the high-intensity linear portions of the measured ion yields, intersect the intensity axis and determine the values of experimental saturation intensities I_{sat}. The laser central wavelength is 800 nm and the pulse duration (full width at half maximum) is 45 fs.

IV. RESULTS AND DISCUSSION

A. Ba and Mg

Figures 2(a) and 2(b) show the measured ion yields as functions of laser intensity at 800 nm for Ba and Mg, respectively. Here the ion yield is the sum of the yields of the singly and doubly charged ions. The predictions from the PPT and ADK theories are presented for comparison. For a direct comparison between the two theories and with the experiment, both simulations have been multiplied by the same factor for each target. Note that the simulations have been integrated numerically over the experimentally determined laser pulse duration and the spatial distribution confined by the 0.5-mm slit. One can find that the PPT simulation is consistent with the experimental data for Ba, while the ADK simulation is much smaller than the data, especially for the lower intensities. This may not be a surprise because the Keldysh parameter γ is varied from 9.44 to 1.49 for the intensities used here. The ADK formula is not expected to be valid for such high values of γ, whereas the PPT theory is applicable.

For Mg, the experiment is performed at higher intensities as compared to Ba. Although we are working in the transition region between TI and MPI mechanisms (γ ranging from 2.14 to 0.84), the ADK simulation is in good agreement with the experiment. The PPT simulation, however, overestimates the experiment. Note that the first-order Coulomb correction factor $(2/En^{*3})^{2n^*}$ is adopted in the PPT simulation [Eq. (2)]. The discrepancy between the PPT result and the experiment possibly implies that this factor is questionable for Mg at 800 nm. In Ref. [47], a more generalized Coulomb correction factor $(2/En^{*3})^{2n^*}(1+2\gamma/e)^{-2n^*}$ was derived. Using this new factor, the PPT simulation shows much better agreement with the data.

To extend the dynamic range of γ, we show the results of Ba and Mg for 1500 nm in Fig. 3. Similar features are found when further increasing the wavelength to 2000 nm (see Fig. 4). The PPT and ADK simulations tend to coincide with each other for these long wavelengths, which is as expected because the ADK formula can be derived from the PPT formula in the limit $\gamma \to 0$. We find good agreement between both simulations and the experiment for Mg. For Ba with relatively larger values of γ, the agreement is still reasonable.

As demonstrated in [44], one main advantage of the experimental configuration using a slit is the convenience of determining the saturation intensity I_{sat} reliably, which is an

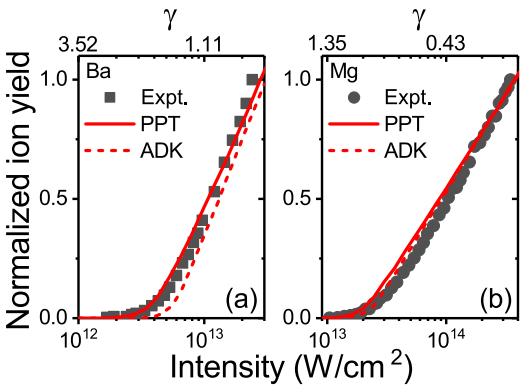

FIG. 3. Same as Fig. 2 but for 1500-nm, 30-fs laser pulses.

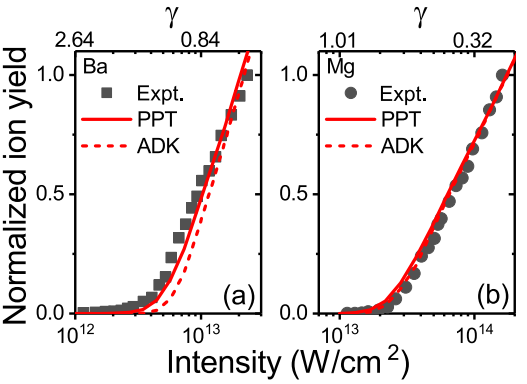

FIG. 4. Same as Fig. 2 but for 2000-nm, 45-fs pulses.

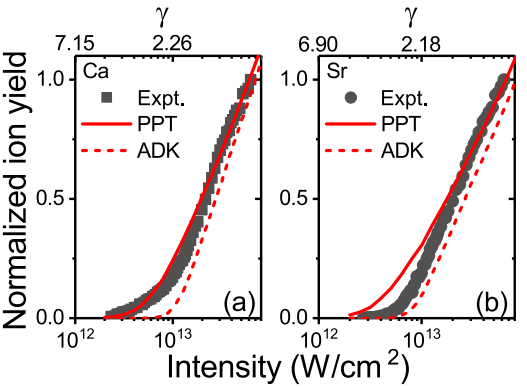

FIG. 5. Same as Fig. 2 but for Ca and Sr results.

TABLE I. Saturation intensities I_{sat} (10^{12} W/cm^2) of Mg and Ba determined from experiment and ADK and PPT theories for different laser parameters. The PPT determined saturation intensity of Mg at 800 nm is obtained from the PPT simulation using the generalized Coulomb correction factor [see the blue line in Fig. 2(b)]. The error bar represents the uncertainty of the intensity determination.

		800 nm, 45 fs			1500 nm, 30 fs			2000 nm, 45 fs		
Atom	IP (eV)	Expt.	ADK	PPT	Expt.	ADK	PPT	Expt.	ADK	PPT
Mg	7.646	28.4 ± 1.4	24.1	23.8	27.1 ± 1.4	24.2	20.2	25.5 ± 1.3	24.1	22.8
Ba	5.212	1.7 ± 0.1	5.9	1.3	4.7 ± 0.2	5.8	4.9	4.6 ± 0.2	5.9	5.8

important physical quantity that shows no dependence on experimental factors such as focusing geometry and detection efficiency. It thus can be compared with theory unambiguously. As shown in Fig. 2, the ion yield reveals a linear dependence on the logarithm of the intensity in the high-intensity region. The saturation intensity can be conveniently extracted from the crossing between the straight line following the linear dependence and the intensity axis [44]. Using the mixture of Ba and Mg in the atomic beam allows us to compare their saturation intensities under identical laser conditions.

A summary of the saturation intensities for Ba and Mg at different wavelengths is shown in Table I. Notably, the experimentally determined I_{sat} of Ba is much smaller than that of Mg for every wavelength. The difference between the ionization potentials of Mg and Ba is 2.43 eV, indicating that at least two more photons are required for the ATI process of Mg with higher ionization potential under identical laser parameters in our work. This reveals that the saturation of ionization becomes much more difficult when several more photons are involved. In general, the PPT and ADK theories agree with the experimental I_{sat} at 800 nm for Ba and Mg, respectively. For long wavelengths, both the PPT and ADK simulations reasonably predict the experimental values of I_{sat} for each atomic species. Interestingly, the experimental I_{sat} of Mg differs slightly when varying the wavelength from 800 nm to 2000 nm, which is well reproduced by the ADK theory. This means that for the transition regime when γ is around 1 for 800 and 1500 nm, the saturation of the ionization of Mg is still well described by the ADK theory. Despite the pulse duration being varied from 45 fs to 30 fs here, the experimental and ADK predicted saturation intensities do not change too much, suggesting a weak dependence of the saturation intensity on the pulse duration with our experimental parameters. The PPT-predicted saturation intensity, however, increases as the wavelength increases. This is because the PPT rate decreases with increasing wavelength. The lower the rate, the higher the intensity required for saturation. For Ba, the experimental saturation intensity for 800 nm is smaller than that for 2000 nm with the same pulse duration by a factor of about 2.7. This indicates that it is easier to saturate the strong-field ionization of Ba when the MPI mechanism is dominant for 800 nm, which is well predicted by the PPT theory. A comparison between the 1500-nm and 2000-nm results within the transition regime (γ is around 1) shows that the experimental and ADK saturation intensities of Ba are almost the same when the pulse duration is increased from 30 fs to 45 fs. This is in accordance with the Mg results at 800 and 1500 nm within similar ranges of γ.

B. Ca and Sr

In this section we further show the comparative study of Ca and Sr. Figure 5 presents the results for 800-nm pulses. The ionization yields show quite similar dependences on the intensity for these two targets because of their close ionization potentials (6.113 eV for Ca and 5.695 eV for Sr). This feature can also be found for the 1500-nm and 2000-nm results shown in Figs. 6 and 7, respectively. Generally, the PPT simulations reproduce the experiments for both Ca and Sr at 800 nm reasonably well and the ADK simulations slightly underestimate. Similar to the Ba and Mg results, for longer wavelengths, both the PPT and ADK predictions are in good agreement with the experiments. Although the Keldysh parameter increases up to ~2.7 when decreasing the wavelength from 2000 nm to 1500 nm, the ADK calculations still reproduce the experimental results for both Ca and Sr very

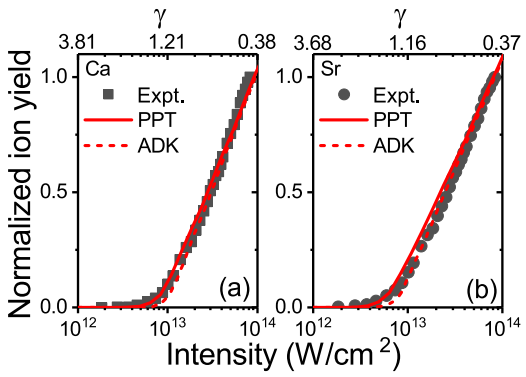

FIG. 6. Same as Fig. 5 but for 1500-nm, 30-fs laser pulses.

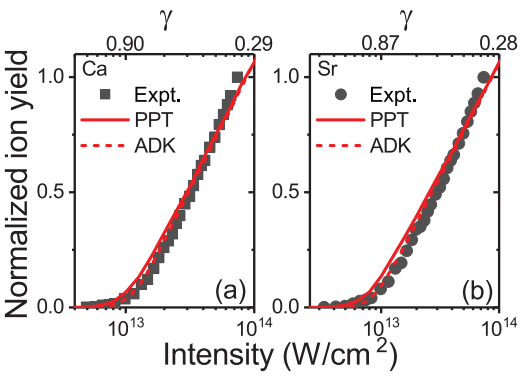

FIG. 7. Same as Fig. 5 but for 2000-nm, 45-fs pulses.

TABLE II. Same as Table I but for the Ca and Sr results.

		800 nm, 45 fs			1500 nm, 30 fs			2000 nm, 45 fs		
Atom	IP (eV)	Expt.	ADK	PPT	Expt.	ADK	PPT	Expt.	ADK	PPT
Ca	6.113	7.6 ± 0.4	10.9	6.8	9.5 ± 0.5	10.0	9.0	11.2 ± 0.6	10.9	10.3
Sr	5.695	6.3 ± 0.3	8.5	5.5	7.6 ± 0.4	8.3	7.1	8.9 ± 0.4	8.5	7.9

well. This indicates the applicability of ADK theory for the intermediate regime between MPI and TI.

In Table II we show the experimentally and theoretically determined saturation intensities for Ca and Sr. The difference between the ionization potentials of Ca and Sr is only 0.42 eV, which is smaller than the photon energy (0.62 eV) for the longest wavelength (2000 nm) used here. This indicates that the minimum number of photons required to overcome the ionization potential is the same for both targets (or just one more photon for Ca) with identical laser parameters. Therefore, the saturation intensity of Ca is close to that of Sr for every wavelength. For both Ca and Sr, the experimental saturation intensity increases with the increase of wavelength, implying that the saturation of ionization becomes slower from MPI to the TI regime. The experimental saturation intensities of Ca and Sr are produced well by the PPT simulations for 800 nm. The ADK simulations slightly overestimate the experimental results. For longer wavelengths, both the PPT and ADK simulations are in excellent agreement with the experiments. In other words, the findings are in accordance with the Ba and Mg results presented above.

In Ref. [19] it was found that the ADK-calculated I_{sat} are significantly smaller than the experiments for several transition metals in the TI regime. This discrepancy has been attributed to the dynamic multielectron polarization effects within those atoms. However, the current study of four alkaline-earth metals with very high static polarizabilities shows no obvious polarization effect based on the overall good agreement between our experiments and the single-active-electron approximation simulations. This generalizes the findings on Mg in Ref. [21] to other alkaline-earth metals. Our work suggests that the polarization effect plays a negligible role in the strong-field-ionization yield of alkaline-earth metals. We hope that this interesting finding could stimulate further theoretical research.

V. CONCLUSION

We have presented a systematic investigation of strong-field ionization of alkaline-earth-metal atoms with intense femtosecond laser pulses from near-infrared to midinfrared wavelengths. Using a small slit to collect only the ionization signals produced within the central portion of the laser focus along the beam, we significantly reduced the focus volume effect and experimentally determined the saturation intensities for different alkaline-earth metals. This allowed us to unambiguously compare our results with strong-field-ionization theories, e.g., PPT and ADK theories, which have been widely used for rare-gas atoms. By mixing different alkaline-earth-metal atoms, we presented a comparative study of the saturation intensities for those atoms. We found overall good agreement between both the measured ionization yield and saturation intensity with the PPT prediction for arbitrary values of the Keldysh parameter γ, while the ADK simulations were consistent with the experiments for the TI regime and also for the transition regime when γ was around 1. This is different from the finding in Ref. [21] that the ADK model significantly underestimates the ionization yield except in the deep-tunneling regime. The ADK rate has been widely used in previous theoretical studies of alkaline-earth metals in the transition regime (see, e.g., Ref. [33]), but experimental verification has been lacking. Here we experimentally proved this point. To summarize, the present work has presented strong-field-ionization experiments of alkaline-earth metals over a broad range of laser parameters and has proved the validity of Keldysh's picture for such atoms. This provides physical insight into the ionization dynamics of atomic species with low ionization potentials and high polarizabilities.

ACKNOWLEDGMENTS

The work was supported by the National Key Research and Development Program of China (Grants No. 2019YFA0307700 and No. 2016YFA0401100) and National Natural Science Foundation of China (Grants No. 11834015, No. 11974380, and No. 11974383).

[1] W. Becker, F. Grasbon, R. Kopold, D. Milosevic, G. Paulus, and H. Walther, Adv. At. Mol. Opt. Phys. **48**, 35 (2002).

[2] P. Agostini and L. F. DiMauro, Adv. At. Mol. Opt. Phys. **61**, 117 (2012).

[3] P. Agostini, F. Fabre, G. Mainfray, G. Petite, and N. K. Rahman, Phys. Rev. Lett. **42**, 1127 (1979).

[4] T. Morishita, A.-T. Le, Z. Chen, and C. D. Lin, Phys. Rev. Lett. **100**, 013903 (2008).

[5] M. Okunishi, T. Morishita, G. Prümper, K. Shimada, C. D. Lin, S. Watanabe, and K. Ueda, Phys. Rev. Lett. **100**, 143001 (2008).

[6] H. Kang, W. Quan, Y. Wang, Z. Lin, M. Wu, H. Liu, X. Liu, B. B. Wang, H. J. Liu, Y. Q. Gu, X. Y. Jia, J. Liu, J. Chen, and Y. Cheng, Phys. Rev. Lett. **104**, 203001 (2010).

[7] G. Paulus, F. Grasbon, H. Walther, P. Villoresi, M. Nisoli, S. Stagira, E. Priori, and S. De Silvestri, Nature (London) **414**, 182 (2001).

[8] L. Keldysh, Sov. Phys. JETP **20**, 1307 (1965).
[9] A. Perelomov, V. Popov, and M. Terent'ev, Sov. Phys. JETP **23**, 924 (1966).
[10] S. Popruzhenko, J. Phys. B **47**, 204001 (2014).
[11] M. Ammosov, N. Delone, and V. Krainov, Sov. Phys. JETP **64**, 1191 (1986).
[12] S. Augst, D. Strickland, D. D. Meyerhofer, S. L. Chin, and J. H. Eberly, Phys. Rev. Lett. **63**, 2212 (1989).
[13] T. Auguste, P. Monot, L.-A. Lompré, G. Mainfray, and C. Manus, J. Phys. B **25**, 4181 (1992).
[14] S. Larochelle, A. Talebpour, and S. Chin, J. Phys. B **31**, 1215 (1998).
[15] C. Guo, Phys. Rev. Lett. **85**, 2276 (2000).
[16] C. Guo and G. N. Gibson, Phys. Rev. A **63**, 040701(R) (2001).
[17] M. B. Gaarde, K. J. Schafer, K. C. Kulander, B. Sheehy, D. Kim, and L. F. DiMauro, Phys. Rev. Lett. **84**, 2822 (2000).
[18] M. Sukharev, E. Charron, and A. Suzor-Weiner, Phys. Rev. A **66**, 053407 (2002).
[19] M. Smits, C. A. de Lange, A. Stolow, and D. M. Rayner, Phys. Rev. Lett. **93**, 213003 (2004).
[20] D. Zille, D. Adolph, M. Möller, A. M. Sayler, and G. G. Paulus, New. J. Phys **20**, 063018 (2018).
[21] Y. H. Lai, J. Xu, U. B. Szafruga, B. K. Talbert, X. Gong, K. Zhang, H. Fuest, M. F. Kling, C. I. Blaga, P. Agostini, and L. F. DiMauro, Phys. Rev. A **96**, 063417 (2017).
[22] M. A. Walker, P. Hansch, and L. D. Van Woerkom, Phys. Rev. A **57**, R701 (1998).
[23] W. Bryan, S. Stebbings, J. McKenna, E. English, M. Suresh, J. Wood, B. Srigengan, I. Turcu, J. Smith, E. Divall *et al.*, Nat. Phys. **2**, 379 (2006).
[24] J. Strohaber and C. J. G. J. Uiterwaal, Phys. Rev. Lett. **100**, 023002 (2008).
[25] P. Wang, A. M. Sayler, K. D. Carnes, B. D. Esry, and I. Ben-Itzhak, Opt. Lett. **30**, 664 (2005).
[26] Y. Albeck, D. M. Kandhasamy, and D. Strasser, Phys. Rev. A **90**, 053422 (2014).
[27] P. Hansch, M. A. Walker, and L. D. Van Woerkom, Phys. Rev. A **54**, R2559 (1996).
[28] A. Talebpour, C. Chien, and S. Chin, J. Phys. B **29**, 5725 (1996).
[29] K. Schafer and K. Kulander, Laser Phys. **7**, 740 (1997).
[30] P. Hansch and L. D. Van Woerkom, Opt. Lett. **21**, 1286 (1996).
[31] E. Papastathopoulos, M. Strehle, and G. Gerber, Chem. Phys. Lett. **408**, 65 (2005).
[32] H.-P. Kang, S.-P. Xu, Y.-L. Wang, S.-G. Yu, X.-Y. Zhao, X.-L. Hao, X.-Y. Lai, T. Pfeifer, X.-J. Liu, J. Chen, Y. Cheng, and Z.-Z. Xu, J. Phys. B **51**, 105601 (2018).
[33] N. I. Shvetsov-Shilovski, M. Lein, and L. B. Madsen, Phys. Rev. A **98**, 023406 (2018).
[34] G. D. Gillen, M. A. Walker, and L. D. Van Woerkom, Phys. Rev. A **64**, 043413 (2001).
[35] N. I. Shvetsov-Shilovski, D. Dimitrovski, and L. B. Madsen, Phys. Rev. A **85**, 023428 (2012).
[36] Y. H. Lai, X. Wang, Y. Li, X. Gong, B. K. Talbert, C. I. Blaga, P. Agostini, and L. F. DiMauro, Phys. Rev. A **101**, 013405 (2020).
[37] P. Agostini and G. Petite, J. Phys. B **17**, L811 (1984).
[38] P. Agostini and G. Petite, J. Phys. B **18**, L281 (1985).
[39] L. F. DiMauro, D. Kim, M. W. Courtney, and M. Anselment, Phys. Rev. A **38**, 2338 (1988).
[40] U. Eichmann, Y. Zhu, and T. Gallagher, J. Phys. B **20**, 4461 (1987).
[41] P. Lambropoulos, X. Tang, P. Agostini, G. Petite, and A. L'Huillier, Phys. Rev. A **38**, 6165 (1988).
[42] J. A. Mitroy, M. S. Safronova, and C. W. Clark, J. Phys. B **43**, 202001 (2010).
[43] S. M. Hankin, D. M. Villeneuve, P. B. Corkum, and D. M. Rayner, Phys. Rev. Lett. **84**, 5082 (2000).
[44] S. M. Hankin, D. M. Villeneuve, P. B. Corkum, and D. M. Rayner, Phys. Rev. A **64**, 013405 (2001).
[45] S. Larochelle, A. Talebpour, and S.-L. Chin, J. Phys. B **31**, 1201 (1998).
[46] A. Perelomov and V. Popov, Sov. Phys. JETP **25**, 336 (1967).
[47] S. V. Popruzhenko, V. D. Mur, V. S. Popov, and D. Bauer, Phys. Rev. Lett. **101**, 193003 (2008).